Computers and Electronics in Agriculture 147 (2018) 34–43

Contents lists available at ScienceDirect

Computers and Electronics in Agriculture

journal homepage: www.elsevier.com/locate/compag

Original papers

Economical thermal-RGB imaging system for monitoring agricultural crops

Yasin Osroosh, Lav R. Khot*, R. Troy Peters

Department of Biological Systems Engineering, Center for Precision and Automated Agricultural Systems, Washington State University, IAREC, Prosser, WA, United States

ARTICLE INFO

Keywords:
Irrigated crops
Center pivot
Thermal-RGB imaging
Image processing algorithm
Crop water status

ABSTRACT

In this study, a low-cost thermal-RGB imager was developed for use in agricultural crop monitoring applications. It is weatherproof, and has a geo-referencing capability along with a power management panel that allows unattended field deployment of the systems for crop monitoring over extended period of time. The imager is made up of single-board Linux-based computer integrated with RGB and thermal imaging modules. The imager can be configured as FTP server to allow data transfer to/from a client computer. Developed was also the custom image-processing algorithm which overlays, aligns thermal and RGB images, and mask for the thermal image to remove the soil background and shaded leaves. The algorithm outputs are the average temperature of sunlit leaves and canopy coverage. Prior to field validation, the performance of ten thermal modules and four fully assembled RGB-thermal imagers were assessed under laboratory conditions. In the spring of 2017, two imagers were mounted on a center pivot retrofitted with Medium Elevation Spray Application (MESA) and Low Elevation Spray Application (LESA) systems in a mint field near Toppenish, WA. The thermal modules showed an accuracy of ± 2.4 °C on average over a range of 0–50 °C of a blackbody target. Although accurate for larger canopies, the imperfect alignment of RGB and thermal images introduced significant errors in the calculations of sunlit leaves surface temperature in images with small canopy coverage. Further investigations revealed that the first peak of thermal image relative frequency histogram could be a more accurate representative of sunlit leaf surface temperature. Overall, the amended image-processing algorithm was able to successfully extract canopy surface temperature and percent canopy cover from a wide range of images captured during the crop growing season. The current design of imager allows for creating a network of imaging units in the field to obtain real-time surface temperature data from plant canopies. The system has the potential to be used for creating evapotranspiration and prescription maps in real-time, and irrigation scheduling.

1. Introduction

Soil water deficit may lead to stomatal closure and elevated canopy temperature in many plant species (Pou et al., 2014). This fact has long been the basis for monitoring plant water status as a surrogate for direct soil moisture measurements (Jackson et al., 1981). The advantage of a thermal-based approach is that it is able to indicate crop health, and detect the effect of salinity and water stress (Pereira et al., 2015). Infrared thermometry-based irrigation scheduling has been shown to be comparable to irrigation scheduling using the most accurate soil water measurement methods in terms of crop water use efficiency (WUE) and crop yields (Colaizzi et al., 2017; O'Shaughnessy et al., 2012, 2015, 2017). Canopy temperature measurements are carried out using either thermal imagers or infrared thermal radiometers with the latter being an economical and simple to use approach (Testi et al., 2008). The limitations of thermal sensors and time limits of aerial-based thermal imagery on one hand, and recent advancements leading to less expensive, high-resolution thermal imagers on the other hand, have encouraged researchers to find a wide range of applications for thermal imagery in agriculture (Khanal et al., 2017; Cohen et al., 2012; Möller et al., 2007). However, complicated image processing requirements and the lack of commercial imagers suitable for continuous field measurements remain a challenge.

An infrared thermometer (IRT) gives an average temperature of plant canopy surface within the sensor's field of view (FOV). Using infrared thermometry in sparse plant canopies, because the soil background and non-transpiring parts of the canopy can interfere with temperature measurements (Wanjura et al., 1984; Blonquist et al., 2009; Osroosh et al., 2016a). Another issue is that both sunlit and shaded leaves may be within the same FOV of the IRT, while the surface temperature of the sunlit leaves better reflect water stress. Shaded parts of canopy may not be good indicators of water stress because lower levels of solar irradiance create low demand for transpiration. These two types of leaves cannot be distinguished using IRT measurements

* Corresponding author.
E-mail addresses: y.osroosh@wsu.edu (Y. Osroosh), lav.khot@wsu.edu (L.R. Khot), troy_peters@wsu.edu (R.T. Peters).

https://doi.org/10.1016/j.compag.2018.02.018
Received 22 August 2017; Received in revised form 8 February 2018; Accepted 11 February 2018

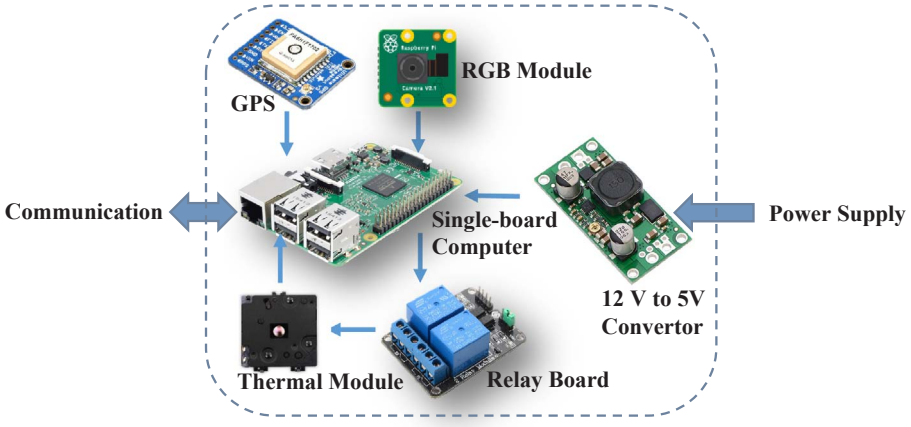

Fig. 1. Electronic components of the thermal-RGB imager. The electronic hardware is comprised of single-board computer, thermal module (radiometric with shutter), RGB camera module, GPS module, and relay board.

alone. Using two IRTs pointed at the same canopy from opposite angles or use of IRTs with a narrow FOV can mitigate such uncertainty (Jones, 1999; Berni et al., 2009; O'Shaughnessy et al., 2011), but does not resolve the issue completely.

Canopy temperature measurements have shown to be correlated well with plant water potential. Cohen et al. (2005) used regression models to correlate the crop water stress index (CWSI) with leaf water potential in cotton. They used thermal imagery to calculate canopy temperatures required for the estimations of the CWSI. Udompetaikul et al. (2011) developed water status classification tools based on empirical relationships among canopy temperature, air temperature, stem water potential and photosynthetically active radiation (PAR) in almond and walnut trees. Similarly, Dhillon et al. (2012, 2014a, 2014b) developed various sensor suites and a continuous leaf monitoring system for the measurements of canopy temperature and crop water status. They evaluated their systems in orchards and vineyards.

Wireless networks of soil, water and plant sensors are increasingly becoming the main method for crop monitoring in agricultural fields, and to schedule irrigation (Coates et al., 2013; O'Shaughnessy et al., 2015; Ojha et al., 2015). Most of the efforts, however, have focused on wireless networks of soil moisture and weather sensors and used with different types of irrigation systems (Stone et al., 1985; Hess, 1996; Abreu and Pereira, 2002). For example, Kim and Evans (2009) used a wireless sensor network (WSN) in a malting barley field to control a site-specific linear-move irrigation system. Different cases of using wireless IRTs have been reported for monitoring canopy surface temperature or irrigation decision-making. Osroosh et al. (2016b) developed a decision support system integrated with a WSN of infrared thermometer, soil moisture and microclimate sensors to automatically schedule irrigation of apple trees. O'Shaughnessy et al. (2013, 2017) used wireless infrared canopy temperature sensors mounted on a center pivot to collect data and create irrigation prescription maps. Colaizzi et al. (2017) used wireless IRTs onboard center pivot to measure canopy surface temperature and estimate crop evapotranspiration. To the best of our knowledge, no thermal imager with the capability of continuous monitoring has been developed and used onboard a moving irrigation system in wired or wireless communication mode.

The emergence of a wide range of open-source hardware and software in recent years has brought many opportunities to the agricultural sector. Many sensing tools, which were once too expensive or too delicate to be deployed in the field, can be developed at a low-cost for field crop monitoring. The emerging thermal sensing technologies are combining robustness, accuracy and low cost. On the other hand, onboard image processing has become possible using low-cost single-board computers like the Raspberry Pi (Raspberry Pi Foundation). Open source image processing libraries such as OpenCV (Open Source Computer Vision) also makes it possible to have most capabilities of a powerful image-processing software like Matlab (MathWorks, Natick, MA) on-board the Raspberry Pi. Existing methods for data transfer, data mining, and computer networking can also be easily used for this purpose. Overall, the above developments are shifting efforts in precision agriculture towards realization of imagery-based continuous crop monitoring systems and control.

Specific objectives of the study were to (i) develop fully automatic crop monitoring and data acquisition system for moving irrigation systems based on thermal-RGB imagery, (ii) develop an image-processing algorithm to extract canopy surface temperature and percent canopy coverage from images, and (iii) calibrate and evaluate the system under laboratory and field conditions. This paper emphasizes the development of the system and presents the preliminary results of assessment in a center pivot-irrigated mint field in the 2017 growing season. Different components of the system, and its performance, benefits and costs are discussed. Combined with microclimate information from an on-site unit, collected data will be used to map crop water stress and crop evapotranspiration (ET_c), which are the subject of another paper.

2. Materials and methods

2.1. Thermal-RGB imager design

Fig. 1 depicts the electronic components of the thermal-RGB imager developed in this study. The electronic hardware is comprised of a Raspberry Pi single-board computer (V3, Raspberry Pi Foundation) as the core, radiometric thermal module with shutter (FLIR Lepton® 2.5, FLIR Systems, Inc., Wilsonville, OR), RGB Raspberry Pi camera module (V2, Raspberry Pi Foundation), GPS module (Ultimate GPS Breakout, Adafruit Industries, New York City, NY), 2-channel relay board (SunFounder, Shenzhen City, Guangdong Province, China), and a precise DC-DC step-up/down voltage convertor (S18V20ALV, Pololu Robotics and Electronics, Las Vegas, NV).

The thermal module has a resolution of 80 (horizontal) × 60 (vertical) pixels, a reported accuracy of ± 5 °C, frame rate of 9 Hz, and a spectral response wavelength range of 8–14 μm. The horizontal field of view (HFOV) of the module is 51°. A breakout board (FLIR Systems, Inc., Wilsonville, OR) with the SPI communication method was used to acquire data from the module. The resolution of the Pi camera is 3280 × 2464 pixels, and has HFOV of 62.2° and vertical field of view (VFOV) of 48.8°. During preliminary experiments with the thermal module, it was noticed that the module would freeze after working for a number of hours. In order to resolve this issue, a relay board was added to the design to reset the module automatically or manually. According

to its documentation, the GPS module has an accuracy of ± 1.8 m under ideal conditions. The GPS module only works with the traditional latitude/longitude/altitude system and provided a real-time clock (RTC) to the Raspberry Pi.

The Raspberry Pi board runs Raspbian Jessie (with PIXEL) as the operating system. We have developed a graphical user interface (GUI) ("ThermoCrop-FST™") in Qt Creator Integrated Development Environment (IDE) (The Qt Company, Santa Clara, CA) using various C and C++ libraries including OpenCV (see Fig. 2). It eases camera settings and allows for real-time monitoring. The main features of the GUI include automatic real-time overlaying of RGB and thermal feeds (if 'RGB Overlay' box is checked), manual capture mode (snapshot), programmable capturing time window, and automatic interval shooting. The imager will capture images automatically at specified time intervals if the 'auto capture' box is checked or takes snapshots manually if the box is unchecked. If the 'auto off' box is checked the application will automatically turn the system off (automatic shutdown). Captured images are processed and stored on a 16-GB SD card. Four images are recorded at each shooting: i) thermal image in binary format, ii) thermal false color image in JPG format, iii) RGB image in JPG format, and iv) automatically aligned RGB and thermal images in JPG format. GPS coordinates are stored in TXT format separately for geotagging images. The available space on the SD card allows for continuously recording images for about 45 days, if configured to acquire data at maximum frequency of one image per min.

2.2. Weatherproof housing

The Raspberry Pi unit can produce a considerable amount of heat depending on CPU usage, which needs to be dissipated. At the same time, dust, humidity and water need to be kept out of the enclosure. To design an appropriate housing, a series of experiments were conducted with various custom-design enclosures. The final enclosure design can be seen in Fig. 3. It is waterproof with the most sensitive points being the thermal and RGB module lenses. The conical frustum-shaped head was added to keep drops of rain from the lenses. One hole was embedded in the housing for the cables and wires to go in or come out. The hole was sealed using duct sealant. The imager housing measures 20 cm in length. The diameter of the widest section is 16 cm and the diameter of the narrowest section is 9 cm. The distance between the lenses is 25 mm. The white enclosure was designed using tinkercad (Autodesk, Inc., San Rafael, CA) and printed using a 3D printer (Ultimaker 3, Ultimaker, Geldermalsen, Netherlands) in our lab. As it can be seen in Fig. 3-b (top view), an external GPS antenna and bullseye level were attached to the imager enclosure. Provided the imager is installed at nadir view, the lenses will be protected from precipitation but not dust

Fig. 2. Graphical user interface (GUI) of the imaging system (ThermoCrop-FST™). The GUI automatically overlays RGB and thermal images in real-time if 'RGB Overlay' box is checked. It can be used for capturing images automatically at specified time intervals (if the 'Auto Capture' box is checked) or taking snapshots manually and setting start and stop capturing times. The imager will automatically shutdown at the 'stop' time if the 'auto off' box is checked.

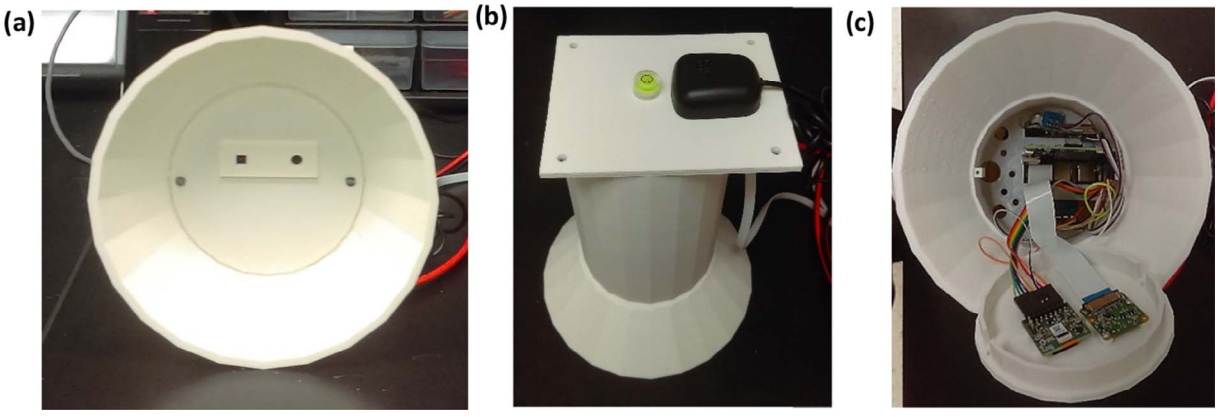

Fig. 3. Thermal-RGB imager enclosure: (a) bottom view (conical frustum-shaped head and camera lenses), (b) top view (GPS antenna and bullseye level), and (c) internal view (compartment for electronic components).

or tiny droplets of water traveling in the wind during an irrigation event. The heat produced by the Pi CPU will also accumulate at the top away from the electronics and dissipated gradually. An internal compartment was designed and 3D printed for securing electronic components inside the enclosure. All the electronics were attached to the compartment except for the camera modules, which were screwed to the cap. The cap was fastened to the body using two small screws and sealed using 100% silicon sealant.

2.3. Power management panel

One of the main challenges with the imagers installed in the field was optimizing their power consumption or managing the power supply for applications requiring continuous monitoring an over extended period. Raspberry Pi 3 draws a relatively high amount of current even under low CPU speeds. Other connected modules and electronic boards, and wireless communications can significantly add to the power consumption. Preliminary measurements showed that the typical current draw of the imager could exceed 500 mA. At this rate, a 7000-mAh acid battery is drawn down to an empty state in about 12 h, assuming an efficiency level of 85%. Thus to manage the power properly, a specific power management panel was designed allowing the imager to be turned on/off at specified times of the day. It is worth mentioning that only images captured at specific times of day (between 10:00am and 2:00 pm) will be useful. Initially, we relied only on a relay board with timer (GERI, Chinese manufacturer); however, it showed a significant daily time drift. We then upgraded the design by adding an Arduino board (model RedBoard, SparkFun Electronics, Boulder, CO) and an ultraprecise real-time clock (ChronoDot, Adafruit Industries, New York City, NY). The ultraprecise timer provided precise time to the Arduino, and the Arduino sent the signal to the relay board to turn the imager on/off. Fig. 4 shows a diagram of the connections between different components of the panel. The panel included a 30 W solar panel (ACOPower, Chino, CA), a charge controller (Sunforce, Montreal West, Canada), two 7000-mAh lead acid batteries (ExpertPower, Paramount, CA) joined in parallel, and an ultraprecise timer as described above.

2.4. Data acquisition and transfer

The imager captures thermal and RGB images and records GPS coordinates at a preset shooting interval. It then processes the images using OpenCV which is embedded in the application. The imager single-board computer is configured as a FTP server, which allows for easy transfer of processed images and other collected data to a remote client computer using the FTP protocol. The connection options are direct using Ethernet cable or wireless using a WiFi access point. Ethernet provides a more reliable and stable connection. Access to the imager application is provided through the Remote Desktop (RD) feature of Windows OS on client computer, and also applications installed on the single-board computer. Although WiFi is available on the Raspberry Pi, it is not reliable and can be very slow. Depending on the distance between nodes, a wireless router can provide internet access to several imagers, or a USB dongle/modem can be used for individual imagers. However, with a predominant network connectivity issue in many agricultural fields these may not be practical. Individual imager is accessed through its unique IP address. The current design of imagers allows for creating a network of imaging units in the field to obtain real-time surface temperature data from plant canopies.

2.5. Lab and field evaluation of the imager

We assembled four units of thermal- RGB imagers and assessed their performance under laboratory conditions. They were run on automatic capturing mode for several months and observed for issues/bugs in the GUI, quality of the images and failure. In order to investigate the reliability of the thermal modules, we also calibrated ten modules using a blackbody calibrator (BB701, Omega Engineering, Inc., Stamford, CT) over a range of 0 to 70 °C. The ambient temperature was 23 ± 0.5 °C throughout the measurements. The duration of each test was less than 15 min and there was no replication. Several thermal modules interfaced to a single-board computer were also run continuously in the lab and monitored independently of the RGB imagers.

In spring of 2017, experiments were conducted in a mint field under

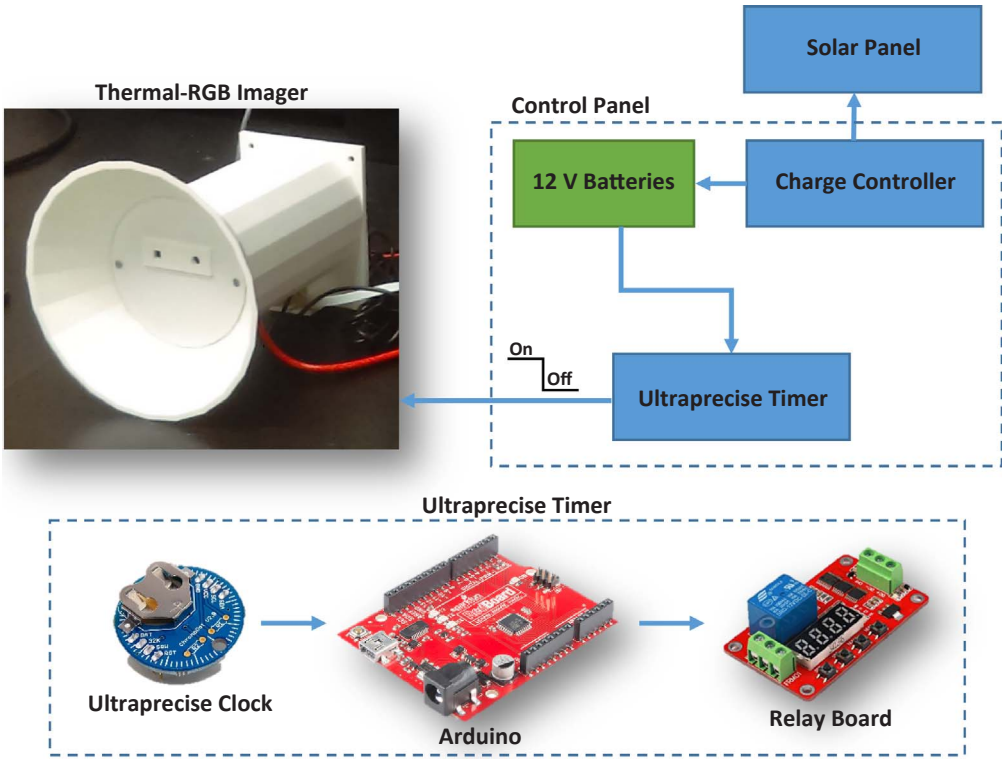

Fig. 4. Diagram of the power management panel. An Arduino-based ultraprecise timer turned the power to the imager on/off at specified times of day.

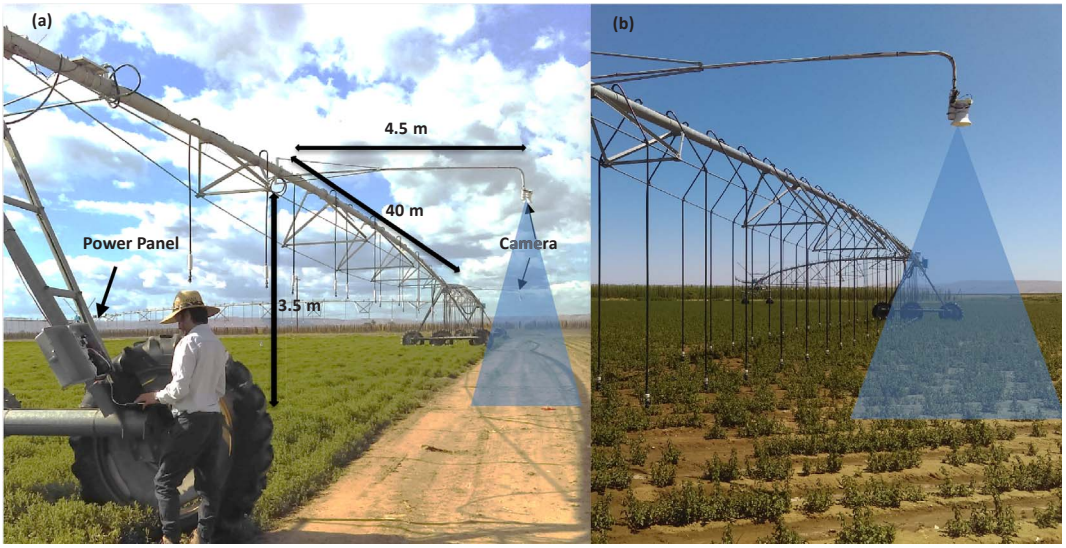

Fig. 5. Installation of thermal-RGB imagers in the mint field (imagers positions and distance from the ground surface and each other): (a) imager mounted on span retrofitted with MESA (close imager), and (b) imager mounted on span retrofitted with LESA. The power management panels were installed next to pivot wheels for easy access. The imagers were attached to boom backs with two support arms.

a center pivot irrigation system near Toppenish, WA (46.38°N, 120.46°W). Two spans of the center pivot were retrofitted with mid-elevation spray application (MESA) and low energy spray application (LESA) irrigation methods (one method per span). One imager was installed on the MESA span and another on the LESA span. The imagers viewed the mint field forward of the irrigations. Imagers positions and distance from the ground surface and each other are illustrated in Fig. 5. Half the field was under peppermint and the rest under spearmint plants. At the beginning of the data collection, the spearmint plants were fully-grown while the peppermints were at early growth stage. The imagers were attached to 4.5-m long boom backs with each having two support arms. The distance between imager lens and bare soil was about 4 m, and from the fully-grown mint canopy surface (in early June 2017) was about 3.5 m. The imagers were located 40 m apart from each other. Considering the thermal module field of view of 51°, it would cover an area of about 10.8 m^2. The area within the FOV was approximately 18 m^2 for the RGB module. The imagers were setup for automatic picture taking at 1 min intervals. Images were captured from 10:00 am–2:00 pm, which is time of maximum stomatal activity for most crops (Jackson et al., 1981; Osroosh et al., 2015b). Based on this shooting interval, the power management panel turned the imager on at 9:50 am and turned it off at 2:10 pm. The imagers were not connected to the Internet, and a Cat 6 ethernet cable was used for connecting a laptop to the imagers.

2.6. Image processing algorithm

The FOV of imagers includes wet/dry soil surface, and sunlit/shaded canopy leaves. An algorithm was developed to automatically detect these components in a RGB image, separate soil background and shaded leaves, and extract sunlit leaves average temperature and percent canopy coverage. The flowchart of the image-processing algorithm is depicted in Fig. 6. The algorithm takes RGB and thermal images, crops, resizes and overlaps images, and creates two types of binary masks. Thermal images are in raw binary data format, which need to be converted to a matrix (80 × 60) of actual temperature values. Factory conversion equation (*temperature* (°C) = $\frac{Pixel\ Value}{100} - 273.15$) and thermal module calibration coefficients determined in the lab are applied to individual pixel raw values to calculate actual temperature (°C). The first mask is created by removing soil background and shaded parts of canopy from the RGB image. The background is then removed from the thermal image by multiplying the binary mask by the thermal image. At the end, the average temperature of sunlit leaves is calculated. The second mask is created using the RGB image and removing only soil background. The resulting image is used to calculate the percent canopy coverage. The process of creating masks involves separating the red, green and blue channels and logical indexing. The green channel is compared with blue and red to segment the image into soil background and canopy. The brightness intensities of red and green channels are the basis for dividing canopy into shaded and sunlit regions. In the calculation of the canopy coverage the latter stage is skipped.

2.7. Data and image analysis

The statistical means used here were (a) the root mean square error (*RMSE*), (b) the mean absolute error (*MAE*), (c) a linear regression between two sets of measurements (calibration), and (d) the standard error of the mean (SE of Mean). The root mean square error was employed as a measure of the variance between n measurements of thermal module (T_{Lep}) and blackbody calibrator (T_{bb}):

$$RMSE = \sqrt{\frac{\sum (T_{Lep} - T_{bb})^2}{n}} \quad (1)$$

The mean absolute error (*MAE*) was also used as a measure of the variance between T_{Lep} and T_{bb}:

$$MAE = \frac{\sum |T_{Lep} - T_{bb}|}{n} \quad (2)$$

The postprocessing of images was conducted in MATLAB (2017Ra, MathWorks, Natick, MA). The 'haversine' formula (van Brummelen, 2013) and lines of VBA code in Microsoft Excel (Microsoft Corporation, Redmond, WA) were used to convert coordinates of two points to distance.

3. Results and discussion

3.1. Laboratory calibration and assessment of thermal modules

Neither the thermal or RGB camera modules have documented information on durability under field conditions. They are very inexpensive yet delicate units. Thus, performance evaluation under field conditions was an important part of this research. At this stage, we were unaware of any effect humidity, dust and temperature fluctuations may

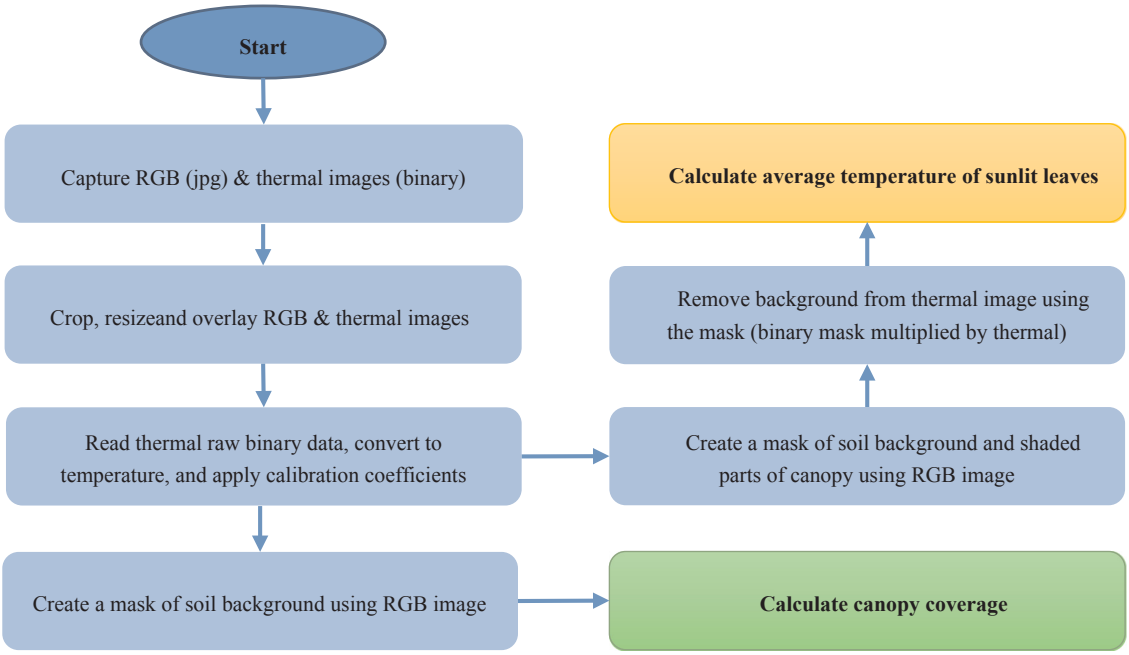

Fig. 6. Flowchart of the image-processing algorithm. The algorithm takes RGB and thermal images, creates binary mask and multiplies it by thermal binary image. The resulting images are used to calculate the average surface temperature of sunlit leaves, and canopy coverage.

have on the performance of the modules long term; however, they survived extremely hot hours of summer in central Washington with no failure. Their low cost allows for affordable replacement in case of malfunctioning. During our lab experiments, we noticed that the thermal module shutter is very susceptible to mechanical failure if mishandled and had one case of failure in the lab. Aside from this, there were no issues with the shutter in the lab or in the field. The thermal module with radiometry is factory-calibrated. According to the documentation, measurements are carried out with a surface in close proximity to the module and 1.0 emissivity. In practice, however, many factors will influence the accuracy of real scene measurements.

Table 1 lists the statistical results for the linear calibration of ten thermal modules in the laboratory at an ambient temperature of 23 ± 0.5 °Cusing the blackbody calibrator. It can be seen that in all cases the coefficient of determination was nearly 1 ($R^2 > 0.999$), and the RMSE, and MAE after calibration were very small ($RMSE < 0.6$ °C; $MAE < 0.5$ °C). The close proximity of RMSE and MAE indicates that the measurements were free of noise (outliers). The average error of thermal modules without calibration was ± 2.4 °C. However, the highest error reached was ± 5.2 °C, which agreed with the value reported by the manufacturer. For some reason, the measurements at temperatures above 50 °C were erroneous. Further investigation revealed that the error was systematic in nature and could be fixed by multiplying -1 to raw sensor readings. It is recommended to run through the calibration process in a room with higher ambient air temperature (e.g. 35 °C) to simulate a range of air temperatures that the sensors will be exposed to during the growing season.

Table 1
Linear calibration of thermal modules (Thermal Module = Slope × BlackBody + Intercept).

Module	Before calibration		After calibration				
	RMSE	MAE	RMSE	MAE	Slope	Intercept	R^2
1[a]	1.5	1.1	0.5	0.4	1.0517	−2.433	0.9992
2[a]	1.6	1.4	0.4	0.3	1.0814	−3.027	0.9995
3	1.2	1.2	0.6	0.5	1.0531	−0.6249	0.9989
4	2.1	1.8	0.3	0.2	1.0833	−3.8876	0.9997
5	1.9	1.5	0.5	0.5	1.1031	−3.4973	0.9991
6	4.4	3.6	0.3	0.2	1.1684	−8.3957	0.9998
7	1.8	1.6	0.4	0.3	1.0915	−1.1042	0.9995
8	2.0	1.8	0.3	0.2	1.1286	−3.0279	0.9997
9	5.2	4.6	0.5	0.4	1.1636	−9.4243	0.9991
10	2.2	2.0	0.4	0.4	1.1164	−4.1138	0.9992
Mean	2.4	2.1	0.4	0.3	1.1041	−3.9536	0.9994

[a]These modules were used in the imagers installed in the field.

3.2. Mint field imaging and data analysis

Sample data mapped using Google Maps™ are illustrated in Fig. 7. The travel speed of the center pivot calculated from the same GPS data sample was 30 m h^{-1} for a travel path of ~74 m. The imager is incapable of detecting center pivot movement, thus it keeps capturing images while the pivot is not traveling. Considering the fact that GPS coordinates are recorded, the application can be modified to capture images based on predefined zones. It may also be possible to use the GPS receiver data to detect movement.

Sample thermal and RGB images captured by the imagers before and after processing are illustrated in Fig. 8. The images are representing fully-grown spearmint with 100% coverage (Fig. 8a), fully-grown spearmint with bare soil in the image (Fig. 8b), and recently planted peppermint plants with bare soil covering most of the image (Fig. 8c). Applying the image-processing algorithm, the average temperature of the sunlit leaves and percent canopy coverage corresponding to the images in Fig. 8a–c were calculated to be 20.7, 18.4 and 40.6 °C, and 100, 96.6 and 15.5%, respectively. The canopy surface temperature in the image with low canopy coverage appeared to be somewhat high. Further inspections revealed that the main source of error was due to slight misalignment of the RGB and thermal images leading to the inclusion of background in the final masked thermal image. This introduced significant error in the calculation of average sunlit leaves surface temperature. The problem was more severe when the plants were sparse and surrounded by hot bare soil. Another source of error was soil background interference with the pixels of thermal image as previously mentioned by O'Shaughnessy et al. (2012, 2015).

The relative frequency histograms of masked thermal images are illustrated in Fig. 9. The images with high canopy coverage (Fig. 9a and b) showed only one peak with a narrow temperature range whereas the

Fig. 7. Satellite view of the mint field and center pivot travel path according to the imager GPS module. The GPS coordinates were recorded consecutively at 157 locations.

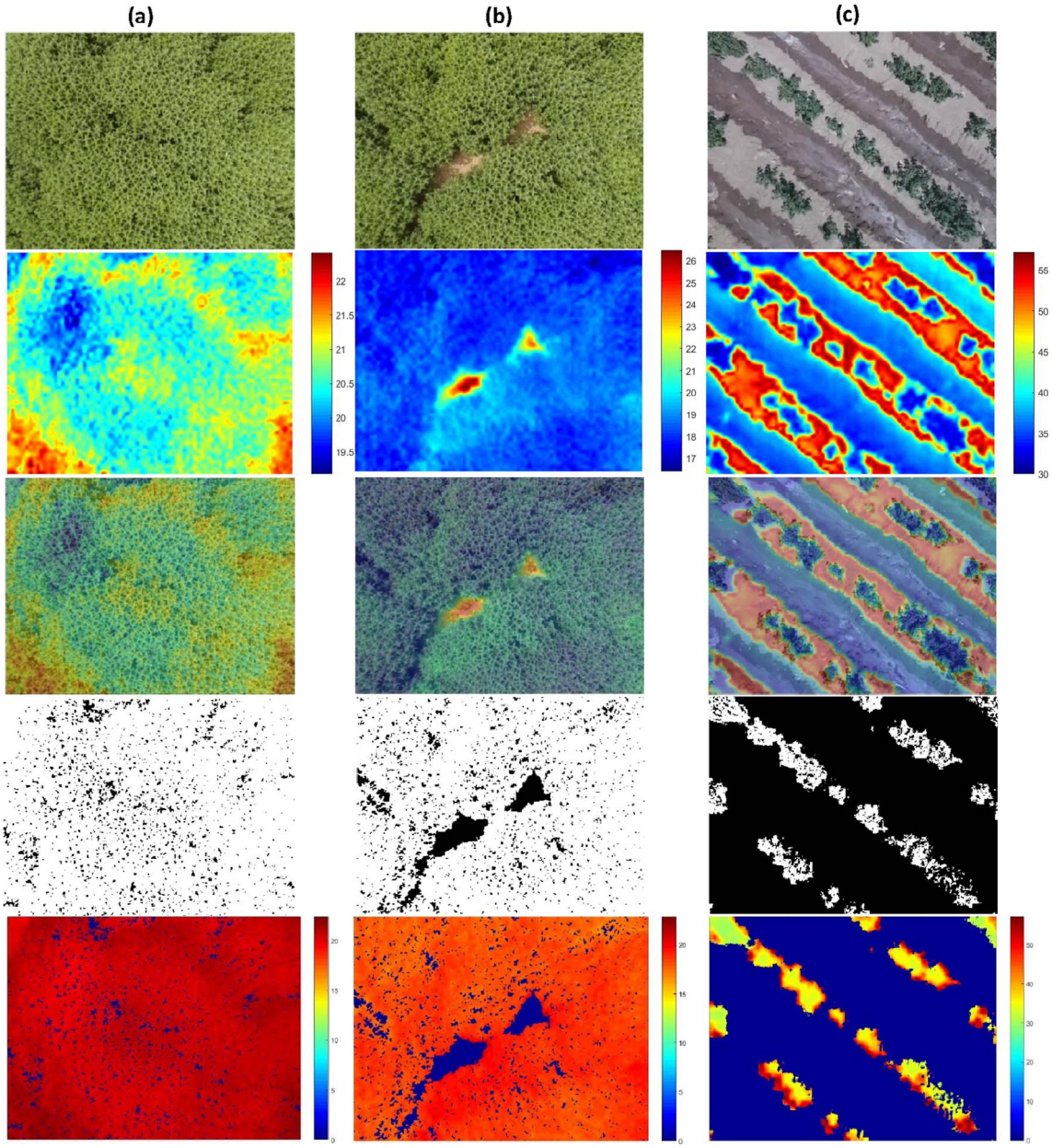

Fig. 8. Sample thermal and RGB images captured by imagers in June and July of 2017 between 10:00am and 2:00 pm, and images as the result of the processing: (a) fully-grown spearmint with 100% coverage, (b) fully-grown spearmint with bare soil in the image, and (c) recently planted peppermint plants. The color bar shows temperature in degree Celsius. Each column of image includes (from top to bottom) RGB image, thermal image, overlayed and resized RGB and thermal images, binary mask, and thermal image multiplied by the binary mask.

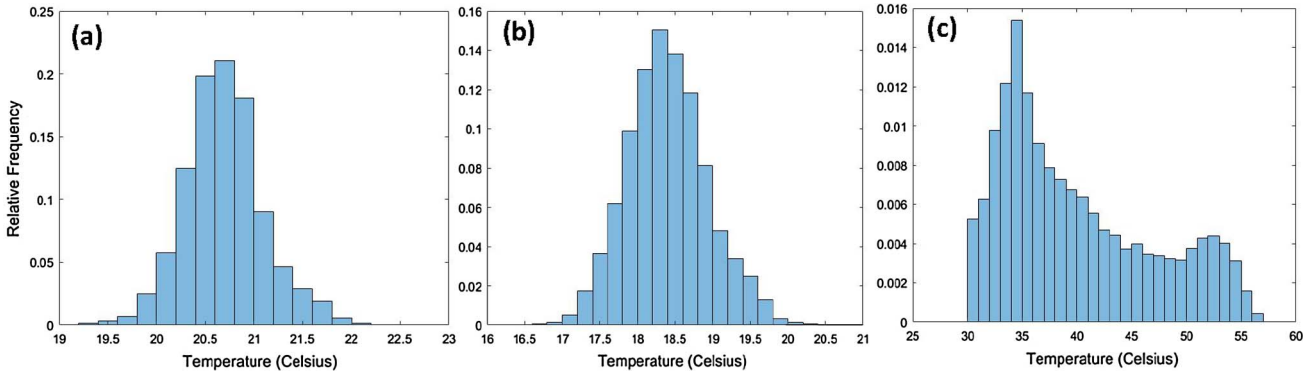

Fig. 9. Relative frequency histogram for sample thermal images in Fig. 8a-c: (a) fully-grown spearmint with 100% coverage, (b) fully-grown spearmint with 96.6% coverage, and (c) recently planted peppermint plants with 15.5% canopy coverage.

Table 2
Extracted surface temperature from sample RGB and thermal images for a variety of canopy coverage.

Sample	Canopy coverage (%)	Mean surface temperature of sunlit leaves (°C)	First peak of relative frequency histogram (°C)
1	100	20.7	20.7
2	96.6	18.4	18.3
3	87.3	33.0	33.5
4	65.4	33.7	32.5
5	15.5	40.6	34.5
6	3.7	36.7	33.4

thermal image of recently planted mints had two significant peaks and a wider range of temperatures. The mean surface temperature of sunlit leaves and canopy cover of six sets of sample images along with the first peak of the relative frequency histogram is listed in Table 2. The mean values and cover percentages were calculated using the original image-processing algorithm. The peak and mean temperature of fully-grown canopies were within ~ 0.1 °C. In the recently planted mints, on the other hand, the difference was 3–5 °C. Inspecting more images (not shown here) proved to be consistent pattern. Looking at the histograms, the values of sunlit canopy leaf surface temperature seem to follow the Gaussian distribution (not statistically tested). The image-processing algorithm was amended according to this finding by replacing the smallest peak temperature (after rounding) with the average temperature of pixels.

3.3. Infrared thermometry versus infrared thermal imagery

Detailed information on the components of the imaging system and their approximate cost are listed in Table 3. Shortcomings and strengths of the traditional IRT-based thermal sensing and our imaging system are also summarized in Table 4. Total cost of building a prototype imager is about $400. An IRT is most often a sensor whose output requires conditioning by a datalogger or reader adding to the expenses in practical applications. Our thermal-RGB imager, contains all the necessary hardware and software for conditioning the thermal module output signal in real-time, processing and recording captured images. This cost is expected to further decrease after commercialization. The cost for the power management panel was about $300, which, depending on the application, may be necessary.

In infrared thermometry, soil background interference with surface temperature readings is a major source of uncertainty (O'Shaughnessy et al., 2012; Osroosh et al., 2015b). Thus, complementary measurements are necessary to distinguish between canopy and soil background. O'Shaughnessy et al. (2015) used an algorithm and simultaneous measurements of thermal IR, NIR and red bands to identify the areas of field covered by either soil or an admixture of soil and plant. The normalized difference vegetation index of <0.25 was the basis for disqualifying a concurrent thermal measurement and not using it to compute the crop water stress index. In the imaging system, combined RGB and thermal imagery allows for removing the soil background and even shaded parts of the canopy effectively, and allows for calculating canopy coverage precisely. When IRTs are used, the only way to account for these is to introduce some assumptions on the percentage of shaded and sunlit leaves, and/or soil background in the modeling

Table 3
Cost for the components of the imaging system in 2016.

Component	Part	Model/Manufacturer	Quantity	Total Price
Thermal-RGB Imager	Single-board computer	Raspberry Pi 3/Raspberry Pi Foundation	1	$40
	SD card	16-GB microSD/Kingston Technology, Fountain Valley, CA	1	$20
	Thermal camera module + breakout board	Lepton 2.5 (radiometric with shutter)/FLIR Systems, Inc., Wilsonville, OR	1	$240
	RGB camera module	Raspberry Pi Camera Module V2/Raspberry Pi Foundation	1	$30
	GPS module + antenna	Ultimate GPS Breakout/Adafruit Industries, New York City, NY	1	$60
	DC-DC convertor	S18V20ALV/Pololu Robotics and Electronics, Las Vegas, NV	1	$17
	Other (cable etc.)			$100
			Total	$407
Power Management Panel	Lead acid battery	12 V, 7 Ah/ExpertPower, Paramount, CA	2	$32
	Solar panel	30 W/ACOPower, Chino, CA	1	$56
	Charge controller	7 A/Sunforce, Montreal West, Canada	1	$20
	Relay cycle timer module	GERI/Chinese manufacturer	1	$16
	Arduino	Redboard/SparkFun Electronics, Boulder, CO	1	$20
	Ultra-precise real-time clock	ChronoDot/Adafruit Industries, New York City, NY	1	$18
	Other (enclosure etc.)			$150
			Total	$310

Table 4
Comparison of thermal sensing using infrared thermometers (IRTs) and thermal imager developed in this study.

System type	Weaknesses	Strengths
IRT-based	- Some models need separate data-logger (additional cost) - Soil background interference with temperature readings - Shaded and sunlit leaves cannot be distinguished - Complementary NDVI or other measurements necessary	- Low maintenance requirements - Low power consumption - High temperature measurement accuracy - Usually rugged, waterproof - Relatively simple algorithms required
Imagery-based	- Complicated image processing algorithms - Complementary RGB imagery is necessary (thermal module resolution is low) - Delicate thermal module - Low temperature measurement accuracy - High power consumption	- Relatively inexpensive - Water proof -Smart (capable of networking) - Embedded data-logging capability - RGB imagery allows for effectively separating soil background and shaded leaves from canopy - Provides canopy temperature map and canopy coverage percentages (after image processing)

(Osroosh et al., 2014, 2015a; Colaizzi et al., 2017). An important difference between IRT and a thermal imager is their accuracy. An IRT can measure surface temperature as accurately as a tenth of a degree while reported accuracy of the best available thermal modules/cameras is around 2 °C. As mentioned earlier, the thermal module used herein has a reported accuracy of ± 5 °Calthough lab calibration of ten sample modules showed an average accuracy of ± 2.5 °C. Power consumption is another concern when using the imager for unattended continuous measurements in the field. The power management panel adds to the total cost. In addition, the number of hours an imager can be used is limited by the power source.

The entire image processing can be done on-board by the imager and there is no need to transfer images to another computer for further processing. ZigBee modules can be added to the design to create a mesh network in the field. In this case, only the resulting data from post processing images are transferred over long distances due to their low speed. In the real-time image-processing scenario, overlaying thermal and RGB images could be carried out by adding a range finding sensor to automatically measure the distance between the imager and canopy surface. Canopy height is also a useful parameter in ET estimations.

As described by Khanal et al. (2017), there are many potential applications of such an imaging system towards plant and fruit stressors monitoring during production. For example, it can be used for tree-fruit frost monitoring for effective actuation of management methods, fruit surface characteristics (temperature, wetness, abiotic/biotic stressors) monitoring, crop pest and disease monitoring, crop transpiration and water stress monitoring, and so on. By combining the imaging system with a microclimate measuring unit, real-time CWSI and evapotranspiration maps can be created. Real-time crop evapotranspiration calculations can be used for creating dynamic prescription maps and irrigation scheduling (Colaizzi et al., 2017). Dynamic prescription map is a relatively new area of research, which currently relies on soil moisture sensors or infrared thermometers abroad center pivot (O'Shaughnessy et al., 2017). Our imaging system can replace/compliment infrared thermometers in such applications and provide higher resolution, and a more accurate map of canopy surface temperature.

4. Conclusion

In this study, we developed a functional thermal-RGB imager and mounted two modules on a center pivot-irrigated mint field in central Washington, United States. To help save power, a power management panel was specifically designed for the imagers to turn them on/off at specified times of day. We also developed image-processing algorithm, which process thermal and RGB images by removing the background from the thermal image, and calculates the surface temperature of sunlit leaves and canopy coverage. Our affordable thermal imager can be used to create a wireless network for high resolution spatial and temporal monitoring of agricultural fields and orchards. Our onboard processing system reduces the traffic on the wireless sensor network. The current design of the imager allows for creating a star network of imaging units in the field to obtain real-time surface temperature data from plant canopies. Therefore, in combination with appropriate models and algorithms, the thermal-RGB imaging system has the potential to be used for creating real-time evapotranspiration and prescription maps, and irrigation scheduling.

Acknowledgements

This material is based upon work that is funded by State of Washington Water Research Center (WRC), United States. This activity was also funded, in part, by National Institute for Food and Agriculture Projects WNP00745. The authors would also like to thank Dr. Muhammad Azeem Khan, Mr. Chongyuan Zhang, Ms. Sanaz Jarolmasjed and Mr. Rajeev R. Sinha of Washington State University, United states for their generous assistance with data collection and analysis.

Appendix A. Supplementary material

Supplementary data associated with this article can be found, in the online version, at http://dx.doi.org/10.1016/j.compag.2018.02.018.

References

Abreu, V.M., Pereira, L.S. (2002). Sprinkler irrigation systems design using ISAMim. ASABE, Paper No. 022254, St. Joseph, MI.
Berni, J.A.J., Zarco-Tejada, P.J., Sepulcre-Canto, G., Fereres, E., Villalobos, F., 2009. Mapping canopy conductance and CWSI in olive orchards using high resolution thermal remote sensing imagery. Remote Sens. Environ. 113, 2380–2388.
Blonquist, J.M., Norman, J.M., Bugbee, B., 2009. Automated measurement of canopy stomatal conductance based on infrared temperature. Agr. Forest. Meteorol. 149, 1931–1945.
Coates, R.W., Delwiche, M.J., Broad, A., Holler, M., 2013. Wireless sensor network with irrigation valve control. Comput. Electron. Agr. 96, 13–22.
Cohen, Y., Alchanatis, V., Meron, M., Saranga, Y., Tsipris, J., 2005. Estimation of leaf water potential by thermal imagery and spatial analysis. J. Exp. Bot. 56 (417), 1843–1852.
Cohen, Y., Alchanatis, V., Prigojin, A., Levi, A., Cohen, Y., 2012. Use of aerial thermal imaging to estimate water status of plam trees. Precision Agric. 13 (1), 123–140.
Colaizzi, P.D., O'Shaughnessy, S.A., Evett, S.R., Mounce, R.B., 2017. Crop evapotranspiration calculation using infrared thermometers aboard center pivots. Agr. Water Manage. 187, 173–189.
Dhillon, R., Udompetaikul, V., Rojo, F., Roach, J., Upadhyaya, S., Slaughter, D., Lampinen, B., Shackel, K., 2012. Detection of Plant Water Stress Using Leaf Temperature Measurements for Vineyard and Nut Crops. Transactions of the ASABE. Available online at: < https://elibrary.asabe.org/azdez.asp?JID=5&AID=42634&CID=dall2012&T=1 > .
Dhillon, R.S., F. Rojo, J. Roach, S. Upadhyaya. 2014a. Handheld sensor suite for plant water status measurements and a comparison of different techniques to measure canopy temperature in orchard crops. ASABE paper 141893976. ASABE St. Joseph, MI 49085.
Dhillon, R., Rojo, F., Roach, J., Upadhyaya, S., Delwiche, M., 2014b. A continuous leaf monitoring system for precision irrigation management in orchard crops. J. Agr.

Machinery Sci. 10 (4), 267–272.
Hess, T., 1996. A microcomputer scheduling program for supplementary irrigation. Comput. Electron. Agr. 15, 233–243.
Jackson, R.D., Idso, S.B., Reginato, R.J., 1981. Canopy temperature as a crop water stress indicator. Water Resour. Res. 17, 1133–1138.
Jones, H.G., 1999. Use of infrared thermometry for estimation of stomatal conductance as a possible aid to irrigation scheduling. Agric. For. Meteorol. 95, 139–149.
Khanal, S., Fulton, J., Shearer, S., 2017. An overview of current and potential applications of thermal remote sensing in precision agriculture. Comput. Electron. Agr. 139, 22–32.
Kim, Y., Evans, R.G., 2009. Software design for wireless sensor-based site-specific irrigation. Comput. Electron. Agr. 66, 159–165.
Möller, M., Alchanatis, V., Cohen, Y., Meron, M., Tsipris, J., Naor, A., Ostrovsky, V., Sprintsin, M., Cohen, S., 2007. Use of thermal and visible imagery for estimating crop water status of irrigated grapevine. J. Exp. Bot. 58, 827–838.
O'Shaughnessy, S.A., Hebel, M.A., Evett, S.R., Colaizzi, 2011. Evaluation of a wireless infrared thermometer with a narrow field of view. Comput. Electron. Agr. 76, 59–68.
O'Shaughnessy, S.A., Evett, S.R., Colaizzi, P.D., Howell, T.A., 2012. A crop water stress index and time threshold for automatic irrigation scheduling of grain sorghum. Agr. Water Manage. 107, 122–132.
O'Shaughnessy, S.A., Evett, S.R., Colaizzi, P.D., Howell, T.A., 2013. Wireless sensor network effectively controls center pivot irrigation of sorghum. Appl. Eng. Agric. 29 (6), 853–864.
O'Shaughnessy, S.A., Evett, S.R., Colaizzi, P.D., 2015. Dynamic prescription maps for site-specific variable rate irrigation of cotton. Agr. Water Manage. 159, 123–138.
O'Shaughnessy, S.A., Andrade, M.A., Evett, S.R., 2017. Using an Integrated Crop Water Stress Index for Irrigation Scheduling of Two Corn Hybrids in a Semi-Arid Region. Sci, Irrig 10.1007/s00271-017-0552-x.
Ojha, T., Misra, S., Raghuwanshi, N.S., 2015. Wireless sensor networks for agriculture: The state-of-the-art in practice and future challenges. Comput. Electron. Agr. 118, 66–84.
Osroosh, Y., Peters, R.T., Campbell, C.S., 2014. Estimating Actual transpiration of apple trees based on infrared thermometry. J. Irrig. Drain. Eng. http://dx.doi.org/10.1061/(ASCE)IR.1943-4774.0000860, 04014084.
Osroosh, Y., Peters, R.T., Campbell, C.S., 2015a. Estimating potential transpiration of apple trees using theoretical non-water-stressed baselines. J. Irrig. Drain. Eng. http://dx.doi.org/10.1061/(ASCE)IR.1943-4774.0000877, 04015009.
Osroosh, Y., Peters, R.T., Campbell, C., Zhang, Q., 2015b. Automatic irrigation scheduling of apple trees using theoretical crop water stress index with an innovative dynamic threshold. Comput. Electron. Agric. 118, 193–203.
Osroosh, Y., Peters, R.T., Campbell, C., 2016a. Daylight crop water stress index for continuous monitoring of water status in apple trees. Irrig. Sci. 34 (3), 209–219.
Osroosh, Y., Peters, R.T., Campbell, C., Zhang, Q., 2016b. Comparison of irrigation automation algorithms for drip-irrigated apple trees. Comput. Electron. Agr. 128, 87–99.
Pereira, L.S., Allen, R.G., Smith, M., Raes, D., 2015. Crop evapotranspiration estimation with FAO56: Past and future. Agr. Water Manage. 147, 4–20.
Pou, A., Diagoa, M.P., Medranob, H., Balujaa, J., Tardaguila, J., 2014. Validation of thermal indices for water status identification in grapevine. Agr. Water Manage. 134, 60–72.
Stone, K.C., Smajstrla, A.G., Zazueta, F.S., 1985. Microcomputer-based data acquisition system for continuous soil water potential measurements. Soil Crop Sci. Soc. Fla. Proc. 44, 49–53.
Testi, L., Goldhamer, D.A., Iniesta, F., Salinas, M., 2008. Crop water stress index is a sensitive water stress indicator in pistachio trees. Irrig. Sci. 26, 395–405.
Udompetaikul, V., Upadhyaya, S.K., Slaughter, D., Lampinen, B., Shackel, K., 2011. Plant Water Stress Detection Using Leaf Temperature and Microclimatic Information. ASABE Meeting Presentation, p. 1111555. Available online at: < http://elibrary.asabe.org/abstract.asp?aid=39304&t=1&redir=aid=39304&redir=[confid=loui2011]&redirType=techpapers.asp&redirType=techpapers.asp > .
van Brummelen, G.R., 2013. Heavenly Mathematics: The Forgotten Art of Spherical Trigonometry. Princeton University Press. ISBN 9780691148922. 0691148929. Retrieved 2015-11-10.
Wanjura, D.F., Kelly, C.A., Wendt, C.W., Hatfield, J.L., 1984. Canopy temperature and water-stress of cotton crops with complete and partial ground cover. Irrig. Sci. 5, 37–46.